Received: 24 September 2021 | Revised: 22 February 2022 | Accepted: 15 April 2022

DOI: 10.33012/navi.530

ORIGINAL ARTICLE

Gain Pattern Reconstruction of GPS Satellite Antennas Using a Global Receiver Network

Gerardo Allende-Alba | **Steffen Thoelert** | **Stefano Caizzone**

Deutsches Zentrum für Luft- und Raumfahrt (DLR), Institute of Communications and Navigation, 82234 Weßling, Germany

RWTH Aachen University, 52062 Aachen, Germany

Correspondence
Gerardo Allende Alba, DLR, Münchener Str. 20, 82234 Weßling, Germany.
Email: gerardo.allendealba@dlr.de

Abstract

For GNSS signal power monitoring systems, the characterization of satellite antennas plays an important role. Recently, gain pattern reconstructions of Galileo satellite antennas have been obtained using single-station observations. However, due to the characteristics of GPS orbits, such an approach is less suitable for GPS satellite antennas. This study introduces a methodology for multi-station satellite antenna gain pattern reconstruction. To overcome the unavailability of receiver antenna gain patterns at the employed stations, a dedicated algorithm is introduced that uses an antenna at a base station to remotely characterize the antennas in network stations. Obtained reconstructions of L1 antenna gain patterns of selected GPS satellites show a consistency at the 0.3–0.4 dB level (95%) with data provided by the manufacturer and better than 0.3 dB (95%) with ground-based observations using a high-gain antenna. The introduced methodology may be employed in the establishment of permanent multi-constellation GNSS signal power monitoring systems.

Keywords

gain pattern estimation, GNSS satellite antenna, GNSS signal power monitoring, GPS, IGS network

1 | INTRODUCTION

The increasing number of GNSS applications with reliability and integrity calls for the implementation and integration of monitoring systems that can be used to improve employed error and threat models (Thombre et al., 2018; Wang & Shen, 2020). For safety-critical applications, integrity protection levels are computed based on the expected characteristics of the error sources in the GNSS positioning system (Walter 2017). Aside from those related to signal propagation, the receiver, and its location, errors for system-based parameters are also included in the positioning error budget. Fundamentally, such parameters include satellite ephemeris, satellite clock errors, and signal biases.

On a routine basis, most of these parameters are estimated by the service provider and delivered to the user via the broadcast navigation message (Langley et al., 2017). However, system-based irregularities in the transmitted signal characteristics that lead to errors in the positioning solution may be more difficult to observe

and/or characterize. Among others, such irregularities include signal deformations that originated at the satellite payload (Thoelert et al., 2020) and those stemming from the satellite antenna (Thoelert et al., 2012). As such, if the impact of such system-based irregularities is not properly analyzed, the computed protection levels for applications with high-integrity requirements may be optimistic. In such a case, the true integrity risk of the system would not be able to be correctly defined (Pullen & Joerger, 2021).

It is in this context that the proper characterization of error sources, threat models, and frequency of event occurrence highlight the need for signal monitoring systems (Lee et al., 2017; Pagot et al., 2016; Spacek & Kovar, 2007). Having a strong focus on navigation system-related parameters, monitoring schemes for high-integrity and safety-of-life applications are built to fulfill, among others, the requirement of detecting low received power levels (FAA, 2005). Through various mechanisms, a low received power has an indirect impact on integrity. For example, monitors to detect interference, cycle slips, ionosphere gradients, and signal deformation, among others, rely on a minimum received power for meeting their respective probabilities of false and missed detection. Similarly, a low received power may indicate the presence of interference and satellite cross-correlation, which in turn also affects satellite acquisition (van Graas & Ugazio, 2021). Monitors configured to detect low power levels must be able to consider such factors affecting the estimation of C/N_0 values. Thus, non-nominal behavior of the satellite hardware should be distinguished as a possible cause (FAA, 2005).

Sudden and major changes in transmission power may be detected by an analysis of received power observations. Events of such characteristics have been noticed in the past for the Galileo In-Orbit Validation (IOV) FM4 and GLONASS R735 satellites (Steigenberger et al., 2018). In contrast, changes in the received power that originate at the transmitting antenna radiation pattern may be subtler and direction dependent, requiring a more involved analysis for their detection. As part of the efforts focused on this kind of analysis, past studies made use of high-gain antennas, in particular, for the evaluation and characterization of the on-orbit performance of antennas of the GIOVE-B satellite (Gatti et al., 2008; Thoelert et al., 2012) and GPS satellites of Block IIR (Marquis & Reigh, 2015).

In a recent contribution, Allende-Alba and Thoelert (2020a) presented a methodology for the reconstruction of satellite antenna gain patterns (hereafter denoted as *s-patterns*) which was also used for a characterization of the on-orbit performance of Galileo satellite antennas (Allende-Alba & Thoelert, 2020b). As a major feature of this method, the use of a low-gain antenna allowed for the concurrent reception of signals from several GNSS satellites, making it apt for signal power monitoring activities. However, being a single station-based approach, its suitability for the analysis of GPS data is very reduced. Due to the GPS orbit repeatability period, the achievable sampling using data from a single station may not be sufficient for a successful s-pattern reconstruction, even after several months of collection. Similarly, the configuration of GPS orbital planes hinders a good distribution of observation points for some satellites in the constellation at any given static location.

The present study extends the methodology of Allende-Alba and Thoelert (2020a) for s-pattern reconstruction by introducing a multi-station approach, which makes it suitable for GPS satellites as well, thus, adding up to recent efforts for the on-orbit characterization of gain patterns of GPS antennas. These include studies focusing on the improvement of the calibration of Level 1B data (Wang et al., 2019a, 2019b) for the Cyclone Global Navigation Satellite System (CYGNSS) mission (Ruf et al., 2013) as well as on the analysis of the space service volume for missions in the geostationary and highly elliptical orbits (Donaldson et al., 2020). Likewise, Marquis

and Reigh (2015) and Marquis (2016) analyzed the performance of antennas of GPS IIR satellites using observations from a high-gain antenna.

Other than such approaches, the method introduced in this study makes use only of observations from a ground network of geodetic-class GNSS receivers and antennas rather than from satellites in Earth's orbit or complex measurement set-ups. Although only a small set of ground stations was considered for this study, the proposed method can be equally applied using larger sets. Given that the speed of s-pattern sampling increases proportionally to the number of well-distributed ground stations under consideration, it is theoretically possible to obtain s-pattern reconstructions that can be used for a rapid analysis of performance-changing events in satellite antennas. Thus, the proposed method may prove to be suitable for the establishment of a permanent global monitoring system for the performance evaluation of GNSS satellite antennas that can provide support to applications with high-integrity requirements.

The first two sections of this paper provide a brief introduction of the main characteristics of GPS satellite antennas and s-pattern sampling for satellites in different orbital planes and, later, compares them to the Galileo case. The advantages of a multi-station approach for this application are then described. In the third section, the main characteristics of the network of GNSS monitoring stations employed in this study are introduced. In the following two sections, the fundamental parts of the proposed methodology are described, including the strategy for receiver antenna gain pattern (hereafter denoted as *r-pattern*) reconstruction and the concurrent processing of observations from multiple stations to obtain estimates of s-patterns. Finally, the last section of the paper is devoted to a discussion of the results. S-patterns of four representative GPS satellites from the latest blocks were reconstructed and the results are compared with theoretical reference patterns from the manufacturer (in the case of IIR satellites). Likewise, ground-based observations using a high-gain antenna are used as an independent assessment of the obtained results for all the satellites under test.

2 | GPS SATELLITE ANTENNAS

As of 2021, the GPS constellation consisted of three main satellite blocks called IIR, IIF, and III. Block IIR is typically divided into sub-blocks IIR-A and IIR-M according to specific satellite features and transmitted signals (IS-GPS-200M, 2021). Manufactured by Lockheed Martin, satellites of Block IIR are equipped with the so-called legacy (first eight vehicles of Block IIR-A) and improved (last four classic vehicles of Block IIR-A and all vehicles of Block IIR-M) antenna panels. Both antenna panel types consist of eight helical elements in a circle together with four helical elements in the center of the panel. The improved panel includes new element designs as well as an optimized alignment (Marquis & Reigh, 2015).

Satellites of Block IIF have been manufactured by Rockwell International (now Boeing; Fisher & Ghassemi, 1999). These satellites are equipped with an antenna panel built upon the model employed in satellites of Blocks II/IIA and also consist of eight helical elements distributed in a circle surrounding four helical elements in the center of the panel (Maqsood, 2017). Satellites of Block III have been manufactured by Lockheed Martin (Marquis & Shaw, 2011). Although the main characteristics of the antenna have not been disclosed at the time of writing, the overall structure should have similar features to the units used for satellites of Block IIR, including the use of eight plus four helical elements.

3 | OBSERVATIONAL GEOMETRY AND PATTERN SAMPLING

The orientation of the transmitting antenna with respect to the receiver is a key factor that drives the process of s-pattern reconstruction. This factor defines the geometry of the observations, which depends upon the satellite attitude model, the station location, and the GNSS constellation design. As a system condition, the latter factor plays a fundamental role in the development of a methodology for s-pattern sampling that enables successful reconstruction (Allende-Alba & Thoelert, 2020a).

The nominal GPS constellation consists of 24 satellites distributed in six orbital planes (identified by the first letters of the alphabet) with an orbital altitude of 20,180 km and a period of revolution of 11 hours, 58 minutes, and 2 seconds, resulting in a ground track repeat cycle of two orbits per sidereal day (Hegarty, 2017). For a given location on Earth (e.g., a monitoring station), the same set of GPS satellites appears in the respective same part of the sky, nominally 4 minutes earlier each day (Agnew & Larson, 2007). The ground track of each visible GPS satellite in a topocentric frame is, thus, repeated every day. In the satellite body-fixed frame (aligned with the yaw-steering frame using the IGS axes convention; Montenbruck et al., 2015), the observation tracks appear just slightly shifted every day. This is a consequence of the dependency of satellite orientation not only on the location of the space vehicle along the orbit, but also on the location of the Sun with respect to the orbital plane (Bar-Sever, 1996).

On the other hand, the nominal Galileo constellation consists of 24 satellites distributed into three orbital planes (also identified by the first letters of the alphabet) with an orbital altitude of 23,222 km and a period of revolution of around 14 hours and 4 minutes, resulting in a ground track repeat cycle of 17 orbits every 10 sidereal days (Falcone et al., 2017). For any visible Galileo satellite, ground tracks are evenly distributed in azimuth in the topocentric frame of a given location on Earth, which repeat approximately every 10 days. In turn, in the satellite body-fixed frame, observation tracks exhibit a more spaced-out distribution among them. In comparison with GPS, this results in a faster and more uniform coverage of ground-based observations that can be used for s-pattern reconstruction (i.e., pattern sampling).

To evaluate and numerically compare the gain pattern coverage for GPS and Galileo satellites, a regular grid of azimuth and nadir coordinates in the satellite body-fixed frame of size 1°×1° is defined. The s-pattern coverage is defined as the ratio between the number of cells with at least one observation and the total number of defined cells. Figure 1 shows the obtained results of different observation periods for nine representative satellites of the GPS and Galileo constellations (one per orbital plane denoted by capital letters) considering the observational geometry defined by one station located in Central Europe using an elevation mask of 0°.

For short observation periods (below 10 days), an s-pattern coverage of around 20% and below was obtained for all satellites. However, a clear improvement for Galileo satellites could be observed already after 20 days of observation. A coverage of around 80% and above was achieved for all Galileo satellites after 100 days of observation, whereas similar levels could only be reached for two of the selected GPS satellites (on planes D and F) after 180 days of observation.

This comparison shows that for a given location on Earth, some GPS satellites will exhibit poor observability for s-pattern generation, even after months of data collection. By itself, this factor alone prevents a successful s-pattern reconstruction for the antennas of such satellites. However, if the observation distribution is also

considered, the unsuitability of GPS satellites using data only from one single location for s-pattern reconstruction (i.e., the single-station approach) is much clearer.

The top panels of Figure 2 depicts the observation tracks in the satellite body-fixed frame considering the same location in Central Europe for the Galileo FM15 (left)

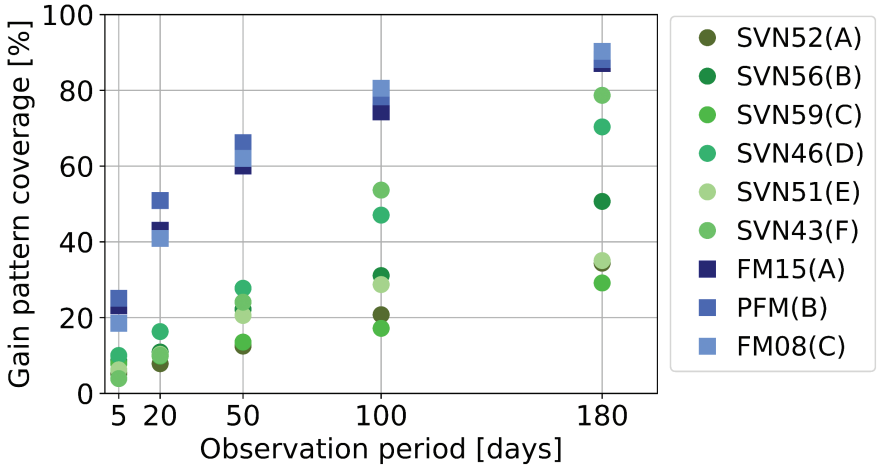

FIGURE 1 Comparison of s-pattern coverages based on a location in Central Europe on different observation periods for satellites of the GPS (green scale) and Galileo (blue scale) constellations

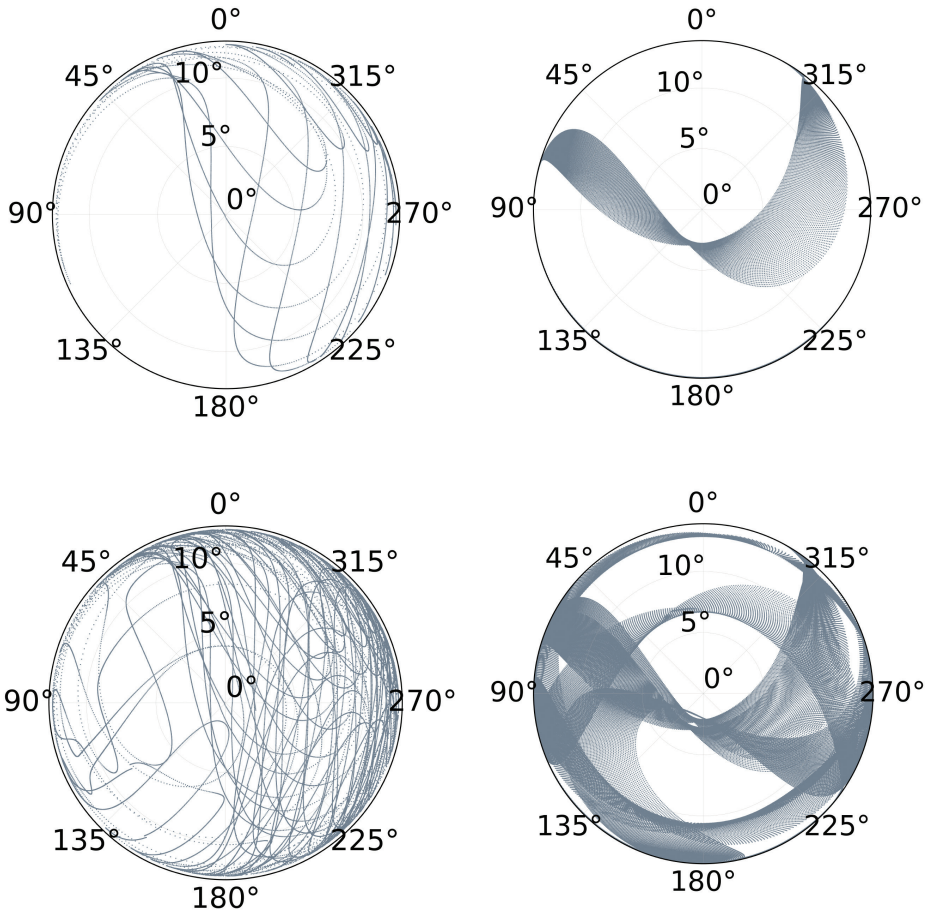

FIGURE 2 S-pattern coverage in the satellite body-fixed frame using 10 and 50 continuous days of data for the Galileo FM15 (left) and GPS SVN46 (right) satellites, respectively

and GPS SVN46 (right) satellites, using 10 and 50 continuous days of data, respectively. Although a similar percentage of s-pattern coverage was obtained (31% for Galileo and 28% for GPS) considering these cases, the contrast in the homogeneity of the observations' distribution is remarkable. For the case of the GPS satellite, large portions of the coordinate grid were not covered and all the observations were concentrated on very specific sections. In contrast, for the Galileo satellite, observations covered a much larger area, allowing for the recovery of mid-scale features after reconstruction in at least one-half of the s-pattern.

The s-pattern coverage for GPS satellites (both in area and distribution of observations) using data from one single location exhibits the need for improving the geometrical diversity of observations for satellite antenna characterization. From the perspective of ground-based systems, such an improvement can be achieved using data from more than one station during the same period of analysis.

The bottom panels of Figure 2 show the resulting s-pattern coverage for the above-mentioned satellites and observation periods, but now considering five stations located in Europe, North America, Antarctica, and the South Pacific. Under these conditions, a better s-pattern coverage of 67% and 57% for Galileo and GPS, respectively, was obtained. The distribution of observations in both cases improved too, as more portions of the s-pattern were covered. Likewise, the inclusion of more stations results in an increased speed of s-pattern sampling, which, for the case of GPS satellites, enables the possibility of recovering more s-pattern features in the final reconstruction.

4 | GNSS RECEIVER NETWORK AND SIGNAL POWER OBSERVATIONS

A key feature of the methodology proposed by Allende-Alba and Thoelert (2020a) is the use of a measurement setup of reduced complexity (including a low-gain antenna). Such a characteristic allows for the proposed methods to be applied to data collected in a typical geodetic-grade GNSS station. In this way, an extension of the aforementioned methodology to a multi-station approach may be readily applicable using data from existing network infrastructure for GNSS signal monitoring (e.g., for scientific purposes).

For this study, data from the GNSS receiver network of the Multi-GNSS Experiment (MGEX) pilot project of the International GNSS Service (IGS) were used (Johnston et al., 2017; Montenbruck et al., 2017). For each station in the network, signal strength observations were provided on the same basis as pseudorange and carrier-phase observations, which guaranteed regular availability of data for the purposes of this study. However, due to the number of stations that are part of the IGS network (as of 2021), the amount of available data represents a challenge for many processing algorithms that make use of such data. For applications such as GNSS orbit and clock determination, some studies apply a pre-processing step for the selection of the best stations in the network (Yang et al., 2019).

A multi-station approach for s-pattern reconstruction can be leveraged in two ways. First, by concurrently processing data from a diversity of stations, the impact of local multipath effects on the final estimates is expected to be reduced. The precision (and robustness) of the solution can thus be increased by employing longer observation periods (although not necessarily continuous days). On the other hand, the use of data from various stations provides an improved diversity of observational geometry. The speed of the s-pattern sampling is thus increased, allowing for the reconstruction of s-patterns with shorter observation periods.

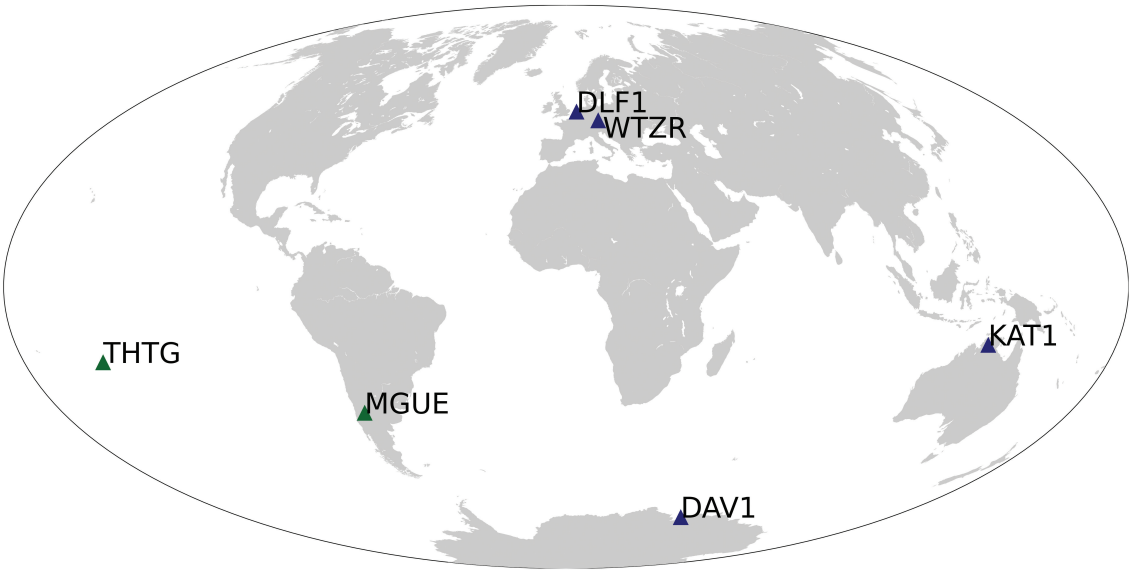

FIGURE 3 Stations from the IGS network used in this study; blue and green markers depict stations of the base and complementary sets, respectively.

TABLE 1
List of Stations of the IGS Network Considered in This Study

ID	COUNTRY/REGION	ANTENNA MODEL
DLF1	Netherlands	Leica AR25 R3
WTZR	Germany	
DAV1	Antarctica	
KAT1	Australia	
THTG	French Polynesia	
MGUE	Argentina	Leica AR25 R4

For each of the aforementioned applications, a selection of the best stations was carried out, although the criteria to classify the stations may have differed (based on data quality, location, continuity of data, frequency of hardware changes, etc.). The multi-station approach applied in this study is mostly focused on the use of large observation spans to attempt the reconstruction of s-patterns of precision. Based on this, the data quality, data availability, and employed receiver antenna model were used as the primary criteria in a heuristic station selection process. Station location was used as a secondary criterion, mostly for the selection of stations that would provide complementary coverage (and s-pattern sampling) for specific satellites and regions.

The location of the resulting station set is shown in Figure 3 and its basic characteristics are summarized in Table 1. In total, four main stations were chosen as the base set for the reconstruction of s-patterns for all the satellites under testing (blue markers in Figure 3). Two additional stations (green markers in Figure 3) were used as a complementary set. In general, given that the impact of different receiver antenna models on the final s-pattern reconstruction has not been analyzed so far, stations with the antenna model Leica AR25 were preferred due to its frequency of occurrence in the IGS network. The evaluation of the impact of using several different receiver antenna models in the present methodology is left for future study.

5 | RECONSTRUCTION OF RECEIVER ANTENNA GAIN PATTERNS

While the usage of stations in the IGS network improves the speed and uniformity of antenna sampling for s-pattern reconstruction, the unavailability of the r-patterns prevents a straightforward extension and application of the scheme proposed by Allende-Alba and Thoelert (2020a). In an effort to overcome this limitation, this study introduces a dedicated algorithm that is devoted to the reconstruction of non-absolute gain patterns of receiver antennas in the selected network stations (shown in Figure 4).

The fundamental idea consists of using a characterized antenna at the base station in order to remotely characterize the antenna in the network stations via a set of satellite antenna gain patterns. In this way, the available information about the antenna in the base station is transferred indirectly to the antennas in other stations. For this study, the base station is located at DLR's Institute of Communication and Navigation in Oberpfaffenhofen, Germany. The observation setup consists of a Septentrio POLARx5R receiver and a Novatel GNSS-750 choke

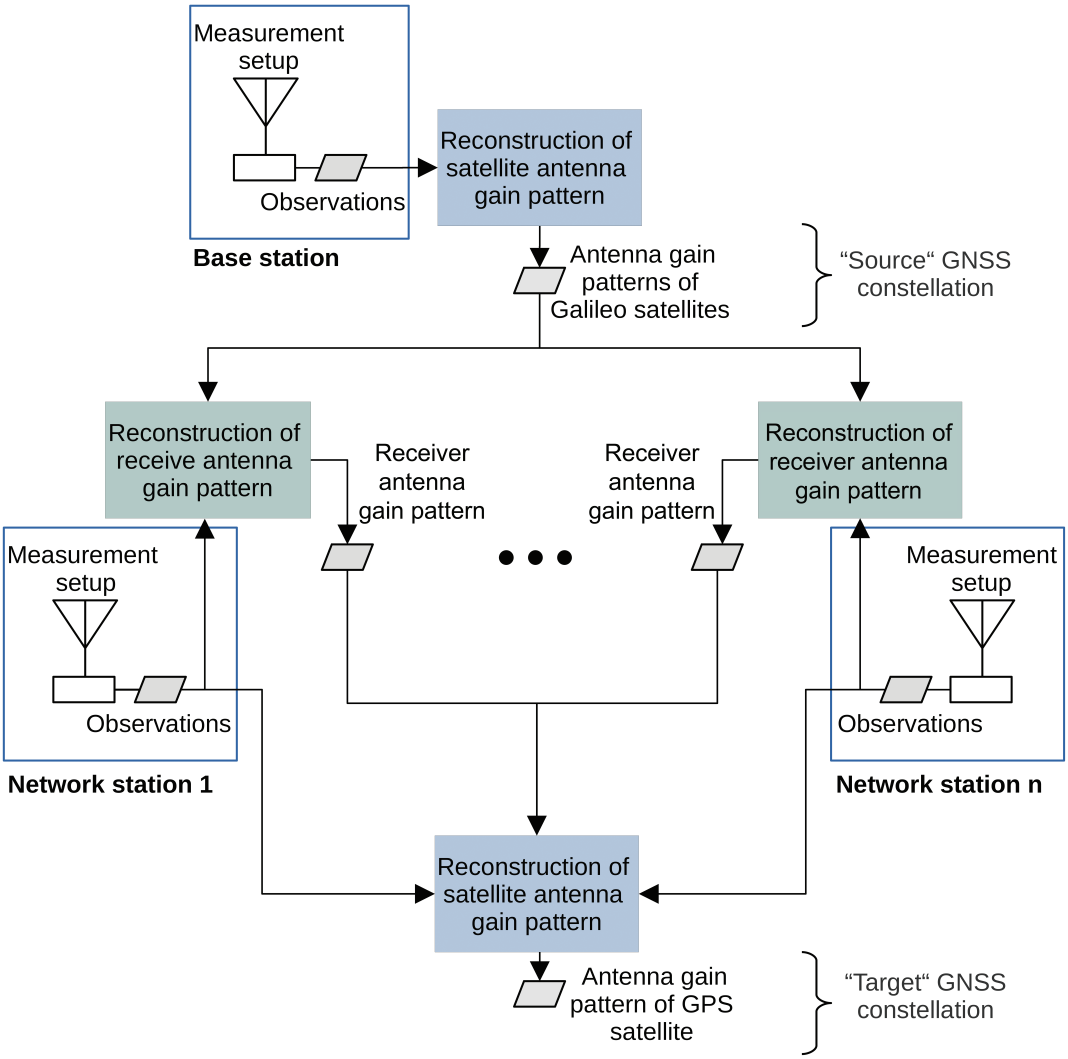

FIGURE 4 Block diagram of the proposed methodology for s-pattern reconstruction using a multi-station approach including a dedicated strategy for r-pattern reconstruction

ring antenna with gain patterns in the L band obtained from measurements in a Starlab anechoic chamber at the Institute for Communication and Navigation of the German Aerospace Center (Caizzone et al., 2021).

In the first step, observations from the base station are used to reconstruct (non-absolute) s-patterns of Galileo satellites in the E1 band as described by Allende-Alba and Thoelert (2020a). Due to the orbital characteristics of the Galileo constellation, the set of all visible satellites at the base station is also visible to the network stations (Falcone et al., 2017). In this way, considering the matching central frequencies of the E1 and L1 bands, the resulting Galileo s-patterns are used as known values in a second step in which gain patterns of receiver antennas of the selected network stations are estimated.

At each epoch, biased receiver antenna gain values $\tilde{g}_r$ at wavelength λ with azimuth ϑ_σ and zenith Θ_σ topocentric coordinates are computed using power observations from Galileo satellite σ as follows:

$$\tilde{g}_r(\vartheta_\sigma, \Theta_\sigma) = \frac{P_{R\sigma}}{P_{T\sigma}\,\bar{g}_\sigma(\varphi_\sigma, \theta_\sigma)}\left(\frac{4\pi\rho_\sigma}{\lambda}\right)^2 \tag{1}$$

using interpolated values of the s-pattern $\bar{g}_\sigma$ with azimuth φ_σ and nadir θ_σ coordinates in the satellite body-fixed frame (aligned with the yaw-steering frame). Orientation vectors and rough estimates of the slant range ρ_σ between station and satellite are computed using broadcast ephemeris data from MGEX (Montenbruck et al., 2017). The transmitted power $P_{T\sigma}$ is assumed as constant during a pass of satellite σ and adjusted using the algorithm proposed by Thoelert et al. (2012) to refer all power levels to a common reference value. Received power $P_{R\sigma}$ values are computed using signal strength (C/N_0) observations. Power-adjusted observation tracks are then used for gain pattern estimation by using a spherical harmonics model:

$$g_r(\vartheta_i, \Theta_i) = \sum_{n=0}^{N}\sum_{m=0}^{n}(a_{nm}\cos(m\vartheta_i) + b_{nm}\sin(m\vartheta_i))\cdot \underline{P}_{nm}\cos\Theta_i \tag{2}$$

where the subscript i denotes individual observation points of all satellites during the period of analysis. The expansion is carried out up to maximum degree N using normalized associated Legendre polynomials $\underline{P}_{nm}$ and spherical wave coefficients a_{nm} and b_{nm} of degree n and order m. Estimates $\hat{a}_{nm}$ and $\hat{b}_{nm}$ are obtained using the computed values of $\tilde{g}_r$ for all epochs and satellites. Lastly, in order to ease the retrieval of values through interpolation for later usage, a final gain pattern $\bar{g}_r(\vartheta_j, \Theta_j)$ is reconstructed using a regular grid of coordinates (ϑ_j, Θ_j).

R-patterns of the selected stations (see Table 2) were reconstructed using 8 days of data from the last week of 2019 and the first week of 2020. For each station, reconstructed s-patterns of six Galileo satellites (two per orbital plane, listed in Table 2) were selected in order to provide a uniform sampling. For the spherical harmonics' expansion, a regular grid of 2°×2° in zenith and azimuth was used as well as a maximum degree $N = 2$ in order to reconstruct mostly high-scale features. Likewise, r-patterns were reconstructed only to up to 80° in zenith coordinates in an effort to try to reduce the impact of the multipath effect in observations of the final estimates.

Figure 5 depicts the zenith-only profiles (median values in azimuth coordinate bins) of reconstructed r-patterns of Leica AR25 antennas of six of the selected

TABLE 2
List of Galileo Satellites Used for R-Pattern Reconstruction

SATELLITE	FM15	FM16	FM3	FM21	FM7	FM13
ORBITAL PLANE	A		B		C	

Note: All satellites belong to the Full Operational Capability (FOC) block

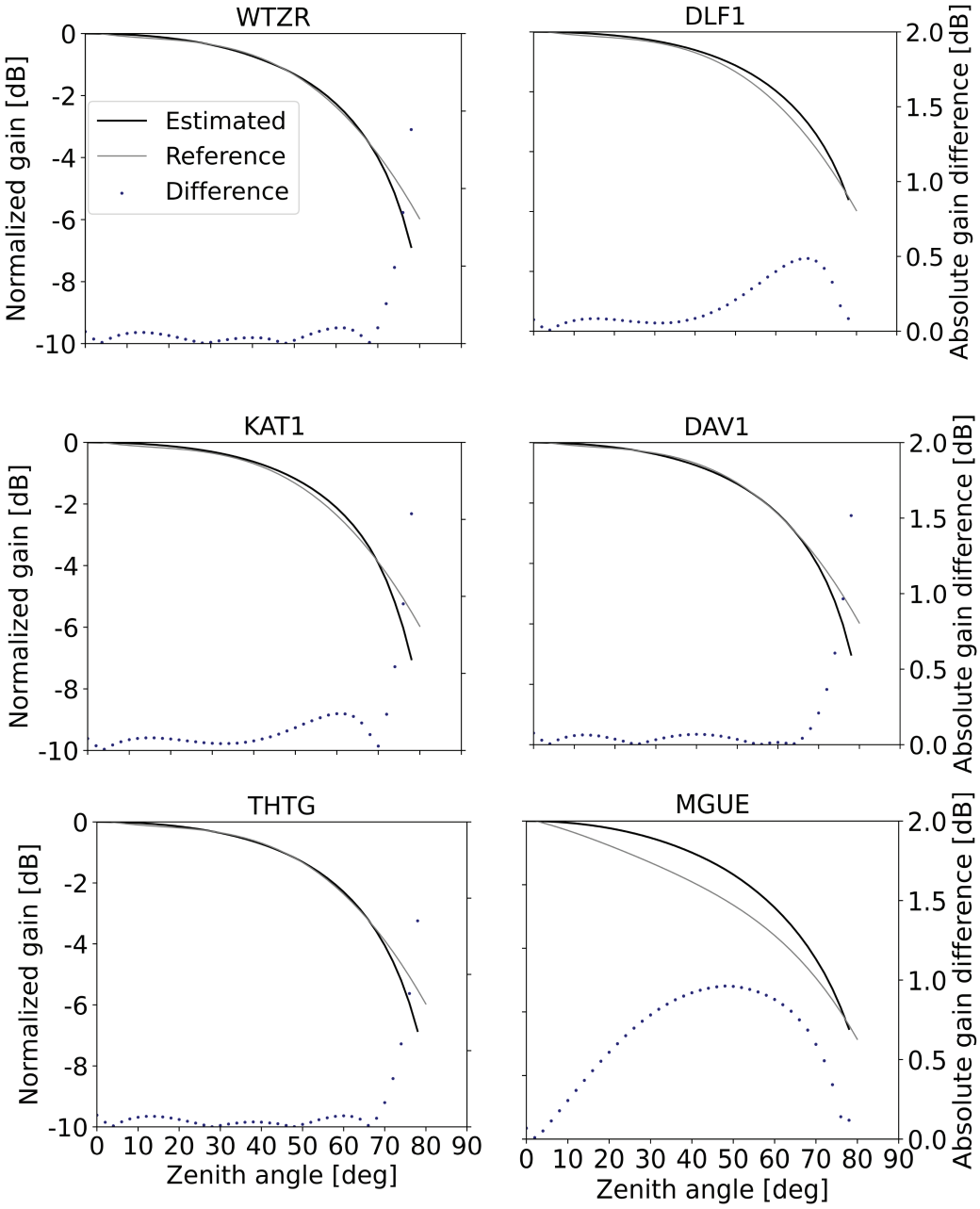

FIGURE 5 Zenith-only profiles (median values in azimuth coordinate bins) of reconstructed r-patterns of Leica AR25 antennas of selected stations of the IGS network (see Table 1)

stations. R-patterns for both subtypes of this antenna model (R3 and R4) measured in the previously mentioned Starlab anechoic chamber were used as reference for the computation of absolute gain differences shown in Figure 5. Both sets of r-patterns were normalized to maximum gain values (close to zenith direction).

For almost all cases, differences below 0.5 dB were obtained for zenith angles up to 70°. For stations WTZR, KAT1, DAV1, and THTG, the largest inconsistences were located close to the horizon, which suggests a higher impact of multipath errors on the final reconstructions. Only for the DLF1 station did all the obtained differences stay below 0.5 dB. The most significant inconsistencies were obtained for the reconstructed r-pattern for the MGUE station, for which differences of up to 1 dB could be observed along all zenith angles. The cause of such large inconsistencies in comparison with the results obtained for the AR25 R4 antenna is still under investigation.

6 | RECONSTRUCTION OF SATELLITE ANTENNA GAIN PATTERNS

With the availability of the respective r-patterns, power observations from the selected network stations were processed in a single scheme to reconstruct the gain pattern of a given GPS satellite s (see Figure 4). At each epoch, the power flux density $\tilde{S}_r$ at location of station r was computed using known receiver antenna gain values and pre-processed signal strength observations using a moving-average filter. Orientation vectors and rough estimates of the slant range ρ_r between satellite and station were computed using broadcast ephemeris products from the MGEX. For each visible station with azimuth φ_r and nadir θ_r coordinates in the satellite body-fixed frame (aligned with the yaw-steering frame), satellite antenna gain values $\tilde{g}_s$ were computed as:

$$\tilde{g}_s(\varphi_r, \theta_r) = \frac{4\pi\rho_r^2 \tilde{S}_r}{P_{Ts}} \tag{3}$$

where the transmitted power P_{Ts} is, again, assumed to be constant during a satellite pass. Power-adjusted observation tracks from all the selected stations in the network and epochs in the selected processing period were used for s-pattern estimation and reconstruction using a spherical harmonics' expansion, similar to the model shown in Equation (2). A final reconstructed gain pattern $\bar{g}_s(\varphi_j, \theta_j)$ was obtained using a regular grid of coordinates (φ_j, θ_j).

7 | RESULTS AND DISCUSSION

S-patterns in the L1 band of four representative GPS satellites from the latest blocks were estimated and reconstructed (see Table 3). While, for all satellites, data from the base station set were used, additional stations were considered for some satellites based on their ground track in order to improve the s-pattern coverage for each case. For satellites SVN63 and SVN74, station THTG was used to extend the base set, whereas for satellite SVN48, station MGUE was selected for this purpose. For satellite SVN43, only the base set was employed.

TABLE 3
List of Selected GPS Satellites Used for S-Pattern Estimation and Reconstruction

SATELLITE	SVN43	SVN48	SVN63	SVN74
BLOCK	IIR-A	IIR-M	IIF	III

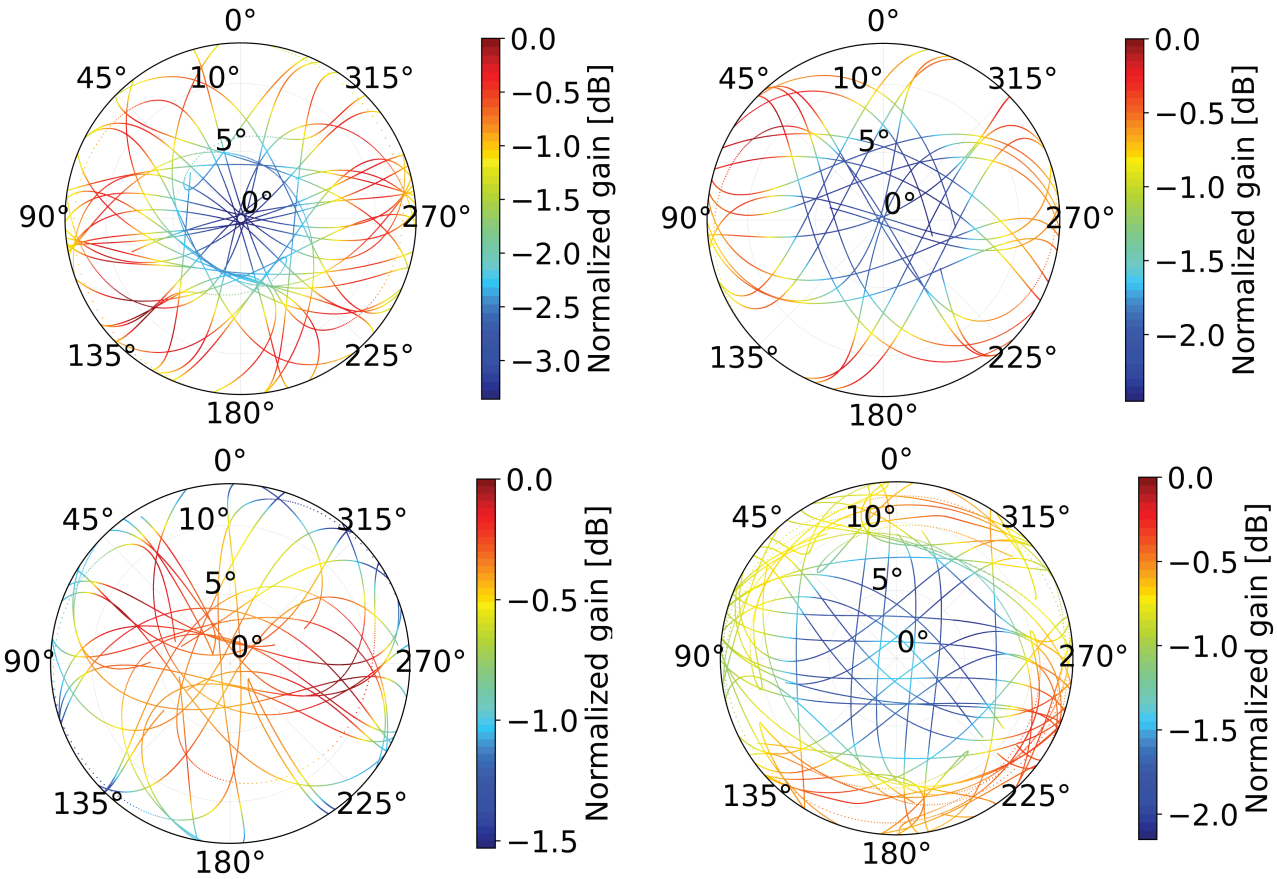

FIGURE 6 Estimated s-patterns of satellites SVN43 (top-left), SVN48 (top-right), SVN63 (bottom-left), and SVN74 (bottom-right)

Data from year 2020 with 45-day steps for satellites SVN48, SVN63, and SVN74 and with 30-day steps for satellite SVN43 were used. Whereas, for satellites SVN43 and SVN74, the whole year's data set was considered, data from January and February were not employed for satellites SVN48 and SVN63 in order to take into account only the so-called Flex Power Mode IV for both satellites, for which the signal L1 C/A was not affected (Steigenberger et al., 2020).

Following the convention used by Allende-Alba and Thoelert (2020a), estimated s-patterns were obtained as a function of observation coordinates using the spherical harmonics' model and estimated spherical wave coefficients. Figure 6 depicts the estimated s-patterns of the four satellite antennas under analysis. Considering the used data time span described before, a coverage of around 60% was achieved for satellite SVN48, whereas for satellites SVN43, SVN63, and SVN74, coverage was around 55%. For all the cases, observations were homogeneously distributed on all sectors with differences only in the data densities along the nadir coordinate due to the considered geometry.

A final reconstruction was obtained using a regular grid of 1°×0.1° in azimuth and nadir coordinates, respectively. Likewise, s-patterns have been reconstructed up to a nadir angle of 12.8° (around 1° away from the edge of nadir) in order to reduce the impact of multipath errors in observations of the final estimates. Figure 7 shows the respective reconstructed s-patterns of the satellites under analysis. Due to the regular distribution of evaluated geometric points, a successful reconstruction provides hints of the main features of the actual s-pattern. As shown by Marquis and Reigh (2015), the legacy antenna panels (used in

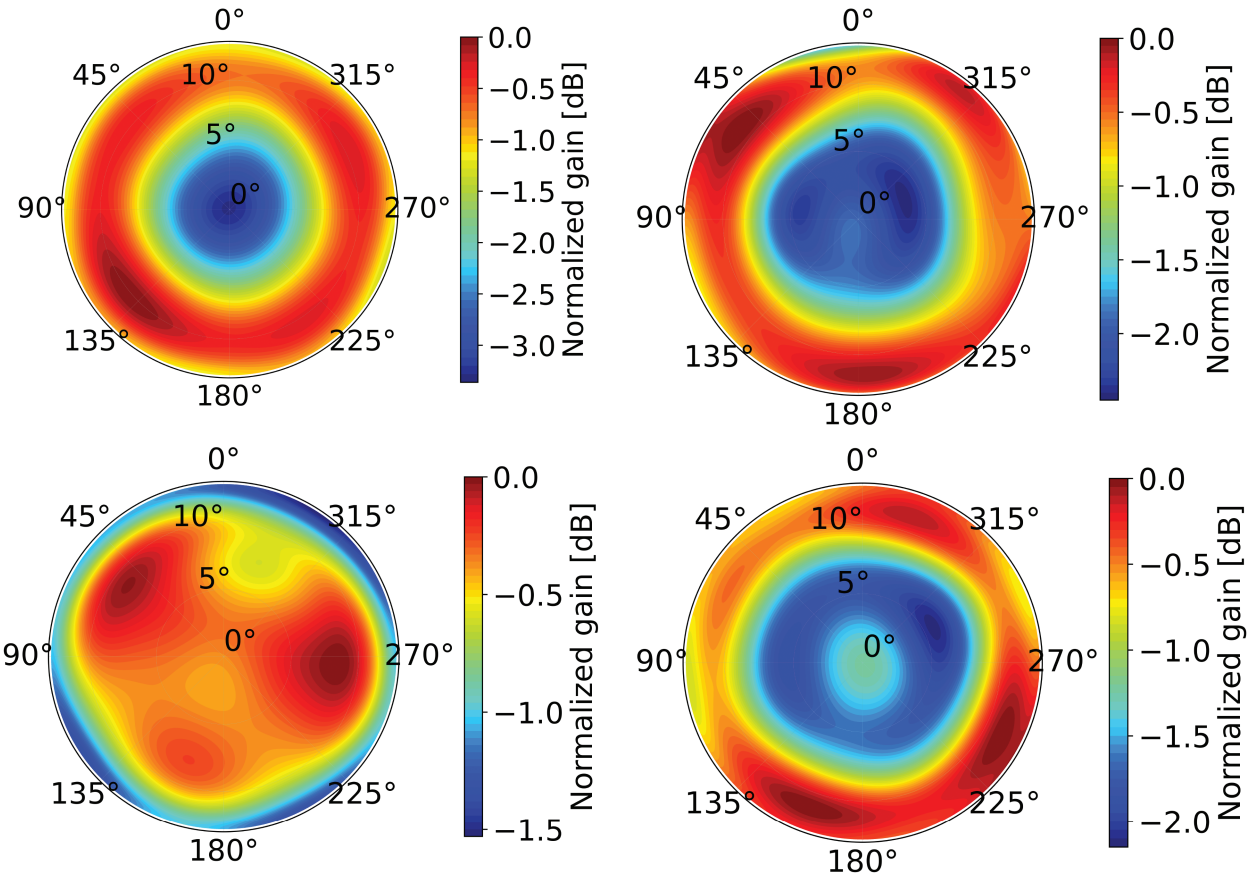

FIGURE 7 Reconstructed s-patterns of satellites SVN43 (top-left), SVN48 (top-right), SVN63 (bottom-left), and SVN74 (bottom-right)

satellite SVN43) and improved antenna panels (used in satellite SVN48) exhibited some differences that can also be observed in the obtained reconstructions shown in Figure 7.

Along the nadir coordinate, the maximum gain values for both antenna panel types were located in the 9° to 10° range, whereas the minimum gain values were located at 0° and around 5° for the legacy and improved antenna panel types, respectively. Similarly, the obtained s-patterns for satellites SVN43 and SVN48 had a range of gain values of around 3.5 dB and 2.5 dB, respectively. For satellite SVN63, the reconstructed s-pattern exhibited a much flatter structure in the 0° to 10° nadir range in comparison to the results obtained from IIR satellites. Above 10°, the gain dropped rapidly, achieving local minimum values close to the edge of nadir. The obtained range of gain values was around 1.5 dB.

These results differ slightly from the s-pattern obtained from measurements of an antenna engineering model originally shown by Fisher and Ghassemi (1999) but, later, displayed more clearly in the study of Steigenberger et al. (2018). In such results, the s-pattern tends to exhibit a less flat structure and a range of gain values around 2 dB. Assuming the validity of the reconstructed s-pattern (as later discussed), this discrepancy may suggest a slightly different than expected on-orbit performance for this satellite antenna. Finally, for satellite SVN74, the reconstructed s-pattern showed maximum and minimum values in the nadir ranges of 10° to 11° and 5° to 6°, respectively. The resulting range of gain values was around 2 dB. The obtained results suggest a similar s-pattern structure of satellites in blocks IIR-M and III, with only minor differences.

7.1 | Evaluation of Results

In order to evaluate the quality of the reconstructed s-patterns shown in Figure 7, two independent approaches were employed in this study. The first one considers s-patterns of satellites of blocks IIR-A and IIR-M measured by Marquis and Reigh (2015) as a theoretical reference. These s-patterns are available for public use (Cozzens, 2020) and consist of measurements (with an uncertainty at the 0.25-dB level) collected before launch on a grid of 10°×2° in azimuth and nadir coordinates, respectively. For this assessment, first mean nadir-only profiles of reconstructed s-patterns were obtained and compared with reference s-patterns as depicted in Figure 8. The reconstructed s-patterns were shifted to match the values of the reference s-pattern at nadir direction. For both cases, the reconstructed profiles exhibited maximum absolute differences below 0.5 dB with respect to the mean observation values for all nadir angles.

In the second part of this assessment, the full normalized reference s-patterns were employed to compute absolute differences with sampled values of reconstructed s-patterns. For this comparison, the coordinates of the reconstructed s-patterns were transformed to match the manufacturer axes convention (Montenbruck et al., 2015).

Figure 9 depicts the differences at the observation points of the reference s-pattern as well as the 95th percentile of the obtained differences at each nadir angle bin. For satellite SVN43, consistencies below 0.4 dB (95%) for almost all nadir angle bins were achieved. Only for the bin close to the edge of nadir a consistency of around 0.5 dB was obtained, with the largest differences located around 270° in azimuth. For the case of satellite SVN48, a consistency below 0.5 dB for all nadir angle bins was achieved. Large differences can be observed in the range 4° to 6° in nadir and close to 0° in the azimuth. Similarly, close to the edge of nadir, maximum differences at the 0.5-dB to 0.6-dB level can be noticed for azimuth angles close to 180°. The overall achieved consistency for both reconstructed s-patterns with their respective references is of 0.33 dB and 0.42 dB (95%) for SVN43 and SVN48, respectively.

In a second independent approach for the evaluation of results, observations from the 30-m dish antenna at the ground station in Weilheim, Germany, have been

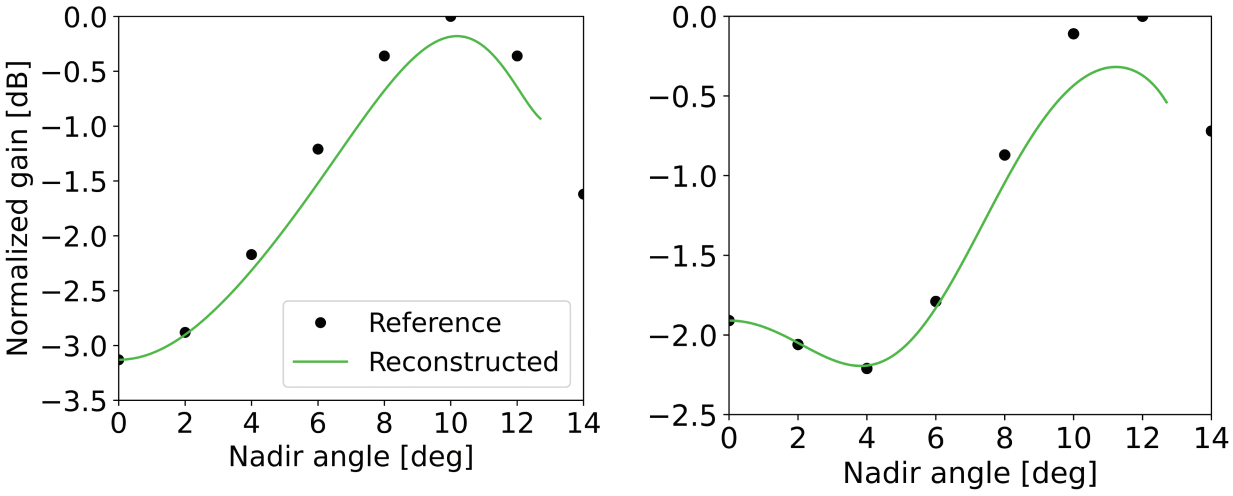

FIGURE 8 Comparison of mean nadir-only pattern profiles of reconstructed s-patterns (green curves) and mean observation values of normalized s-patterns (black dots) published by Lockheed Martin for satellites SVN43 (left) and SVN48 (right)

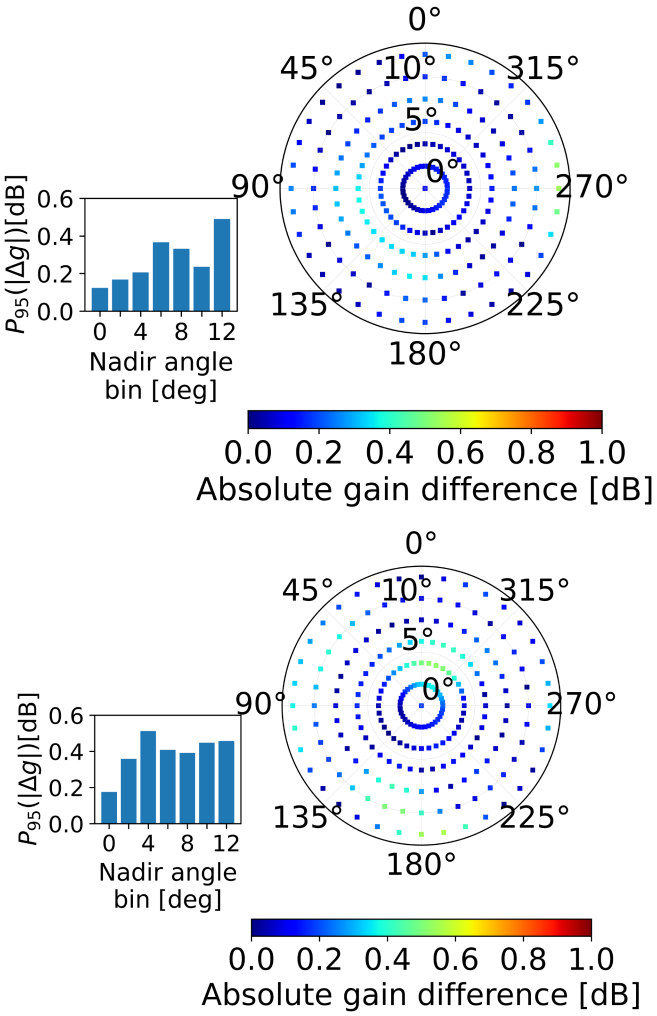

FIGURE 9 Comparison of sampled reconstructed s-pattern values and s-pattern observations published by Lockheed Martin for satellites SVN43 (top) and SVN48 (bottom); for each case, the 95th percentiles of absolute gain differences for each nadir bin of observations are also depicted

TABLE 4
Satellite Passes Observed in Weilheim

SATELLITE	SVN43	SVN48	SVN63	SVN74
DATE	18.11.2016	05.07.2017	22.02.2020	15.01.2019

used as reference values. The antenna, under operation by the German Aerospace Center (DLR), has a gain of around 50 dBi in the L band and an achieved observation precision nowadays of around 0.2 dB after the assessment of calibration uncertainties carried out by Thoelert et al. (2009). For this evaluation, the location of observations from the high-gain antenna were used to extract a cut through the reconstructed s-pattern, using a tolerance search box of 0.15° and 0.5° in nadir and azimuth coordinates, respectively. For each satellite, available data corresponding to one satellite pass collected at different periods were used for this assessment, as seen in Table 4.

Figure 10 depicts the normalized observations from the high-gain antenna and the cut through the reconstructed s-patterns for the four satellites under analysis. For completeness, for satellites SVN43 and SVN48, mean nadir-only profile points

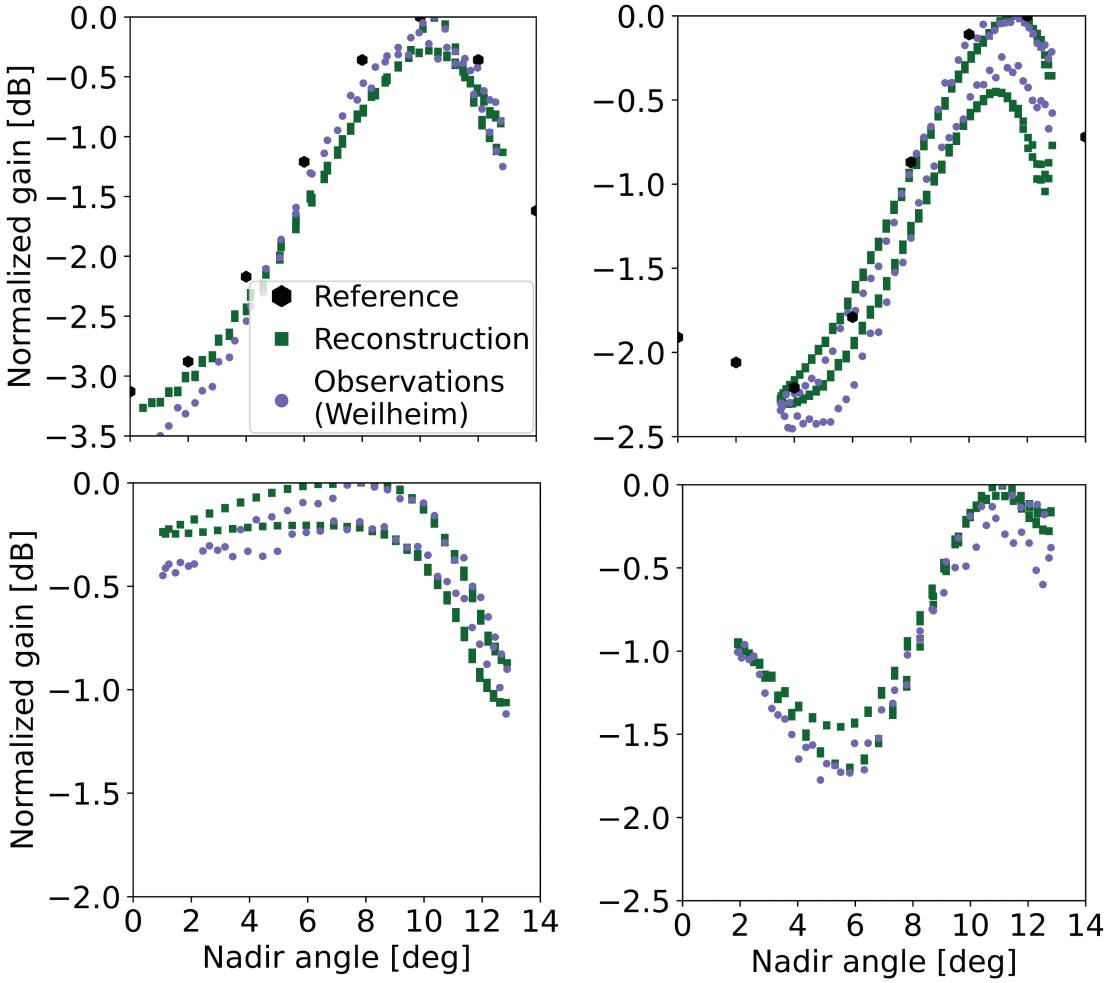

FIGURE 10 Comparison of reconstructed s-pattern cuts with observations from the high-gain antenna in Weilheim and available reference values from Lockheed Martin for satellites SVN43 (top-left), SVN48 (top-right), SVN63 (bottom-left), and SVN74 (bottom-right)

from reference patterns from Lockheed Martin are also depicted (two upper plots in Figure 10).

Except for satellite SVN74, all s-patterns exhibited asymmetries along the azimuth coordinate at the 0.3-dB to 0.4-dB level, which are visible in both the observations and the reconstructions. Slightly smaller asymmetries at the 0.2-dB to 0.3-dB level in the s-pattern for satellite SVN74 were mostly visible in the high-gain antenna observations but less clear in the reconstruction. For satellite SVN43, the reconstruction and reference values appeared to follow a consistent profile for nadir angles 0° through 6°, which was also the case for the high-gain antenna observations but only for nadir angles 4° through 6°. The azimuthal asymmetry close to nadir angles 10° through 12° shown in the observations seems to be well reproduced in the reconstruction. Considering the time difference of around 4 years between the date of observations (see Table 4) and the employed data set for reconstruction, these results suggest a highly stable performance of the antenna under analysis.

For the case of satellite SVN48, reference values, observations, and reconstruction exhibited a consistent profile only for one section of the pattern. As already hinted in the results shown in Figure 7, the s-pattern for satellite SVN63 appears to be flatter than its counterparts from the other blocks. Such a characteristic is also

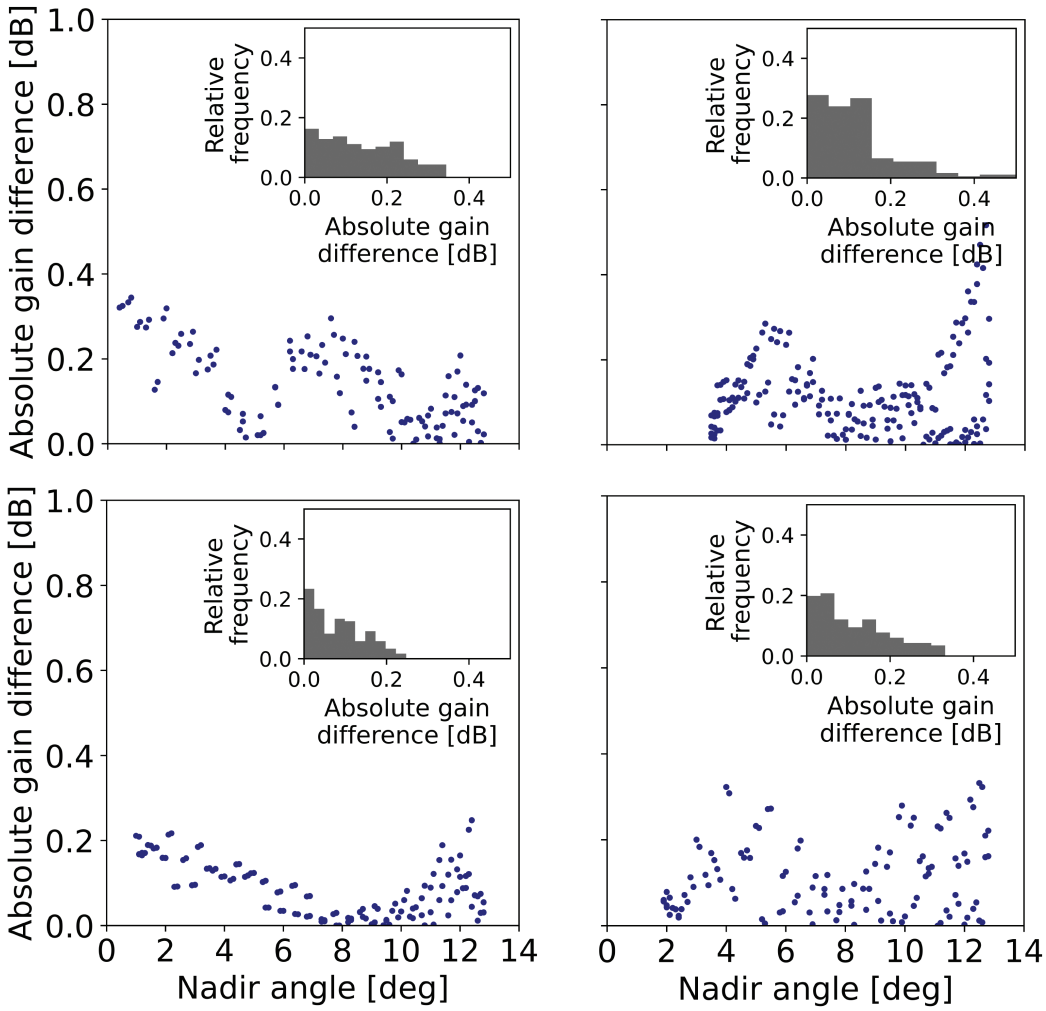

FIGURE 11 Evaluation of reconstructed s-pattern cuts using observations from the high-gain antenna in Weilheim as reference for satellites SVN43 (top-left), SVN48 (top-right), SVN63 (bottom-left), and SVN74 (bottom-right)

exhibited both in the observations and the reconstruction. Other than the results for Galileo satellites obtained by Allende-Alba and Thoelert (2020a), the s-pattern profiles depicted in Figure 10 exhibit lower variations close to the edge of nadir. Due to the use of different observation geometries in the multi-station approach, these results suggest an effective reduction of the impact of multipath errors in signal strength measurements on the final estimates.

To quantitatively evaluate the consistency among observations from Weilheim and the reconstructed s-patterns, absolute differences of the two sets of points were obtained (shown in Figure 11 for the four satellites under consideration). For each case, the frequency distribution of differences is also depicted. For both satellites SVN43 and SVN48, a consistency of 0.29 dB (95%) was achieved. For satellite SVN48, the largest differences were located in the 4° to 7° range as well as close to the edge of nadir, which may be attributable to a slightly tilted leveling of the reconstructed s-pattern. A similar apparent tilt in the s-patterns of satellites SVN43 and SVN63 may be a major cause of the higher differences close to the nadir direction. For satellite SVN63, the differences in the 6° to 10° range stay below 0.1 dB and increase toward the edge of nadir, staying below 0.2 dB for most of the comparison points. For this satellite, an overall consistency of 0.19 dB (95%) was obtained.

Finally, for satellite SVN74, a certain uniformity of differences along nadir angles could be observed, which hints at a proper leveling of the reconstructed s-pattern as well as a lower impact of multipath errors close to the edge of nadir. As a result, a consistency of 0.27 dB (95%) was achieved.

In general, the obtained results suggest the feasibility of the multi-station approach for the reconstruction of s-patterns. Aside from providing a solution to the s-pattern coverage problem for the case of the GPS constellation, the multi-station approach offers benefits to the overall methodology such as an effective reduction of multipath errors in signal strength observations on the final estimates, as suggested by the obtained results depicted in Figure 10. However, the use of data from different stations with heterogenous characteristics and performances pose extra challenges that must be tackled for an improved robustness of the methodology.

In particular, the slight tilt exhibited by the reconstructed s-patterns for satellites SVN48 and SVN63 with respect to observations from Weilheim might be attributed to small errors in the results from the employed power leveling algorithm. Indeed, given the big influence of quality of observations on the correct estimation of power scaling factors, any abnormal sets of observations from any of the stations under consideration (which may be only due to a temporal issue) may have an impact on the final reconstruction, in particular, on the resulting pattern tilt.

8 | CONCLUSION

This study presented a methodology for satellite gain pattern reconstruction based on observations from a network of ground stations. The strategy is particularly suitable for satellites in the GPS constellation given that it provides a solution to the pattern coverage problem through the concurrent use of data from ground stations distributed around the globe. The study focused on patterns in the L1/E1 band, although the presented algorithm can also be applied to the reconstruction of GPS satellite antenna gain patterns in the L5/E5a band.

In the first step, a dedicated algorithm for the reconstruction of gain patterns of receiver antennas of ground stations in the IGS network was introduced in this study. The main idea of such an algorithm consists of using a characterized antenna at the base station in order to remotely characterize the antenna in the network stations via a set of satellite antenna gain patterns. For this purpose, gain patterns of selected Galileo satellites were used.

In the second step, with available receiver antenna gain patterns, signal strength observations from all selected stations were concurrently processed to reconstruct the gain pattern for a particular GPS satellite. To test the presented methodology, gain patterns of four representative GPS satellites were estimated and reconstructed. For satellites SVN43 and SVN48, a comparison of the obtained reconstructions with reference patterns from the manufacturer yields a consistency at the 0.33-dB and 0.42-dB level (95%), respectively. As an independent assessment strategy, observations from the 30-m antenna at the Weilheim ground station in Germany were employed. For all the satellites under testing, a consistency with such observations of better than 0.3 dB (95%) was obtained.

One of the main features of the presented methodology is that it can be regarded as a general approach that is independent of observations taken in space platforms (i.e., satellites in low Earth orbits and geostationary orbits). Being mission- and application-independent, this methodology can be used for the reconstruction of antenna gain patterns of satellites of the GLONASS, Galileo, and BeiDou

constellations, as well. The introduced strategy for receiver antenna gain pattern reconstruction enables (theoretically) the use of data gathered in any geodetic-class monitoring station, regardless of the availability of characterized gain patterns of receiver antennas. In this way, the methodology proposed in this study may be suitable for the establishment of a permanent multi-constellation multi-frequency GNSS signal power and satellite antenna monitoring system that may provide support for safety-critical applications.

ACKNOWLEDGEMENTS

This study makes use of broadcast ephemeris and observation data from the multi-GNSS experiment from the International GNSS Service. The support of all the involved institutions and analysis centers is gratefully acknowledged. The authors are also grateful to Lockheed Martin for making publicly available antenna gain patterns of GPS satellites of blocks IIR-A and IIR-M.

REFERENCES

Agnew, D. C., & Larson, K. M., (2007). Finding the repeat times of the GPS constellation. *GPS Solutions,* 11, 71–76. https://doi.org/10.1007/s10291-006-0038-4

Allende-Alba, G., Thoelert, S. (2020a). Reconstructing antenna gain patterns of Galileo satellites for signal power monitoring. *GPS Solutions*, 24, 22. https://doi.org/10.1007/s10291-019-0937-9

Allende-Alba, G., & Thoelert S. (2020b). An analysis of the on-orbit performance of Galileo satellite antennas using reconstructed gain patterns. *GPS Solutions,* 24, 79. https://doi.org/10.1007/s10291-020-00991-2

Bar-Sever, Y. E. (1996). A new model for GPS yaw attitude. *Journal of Geodesy,* 70(11), 714–723. https://doi.org/10.1007/BF00867149

Bedford, L., Brown, N., & Walford, J. (2009). New 3D four constellation high performance wideband choke ring antenna. *Proc. of the 2009 International Technical Meeting of the Institute of Navigation,* Anaheim, CA, 829–835. https://www.ion.org/publications/abstract.cfm?articleID=8365

Caizzone, S., Schöenfeldt, M., Elmarissi, W., & Circiu, M. -S. (2021). Antennas as precise sensors for GNSS reference stations and high-performances PNT applications on Earth and in space. *Sensors*, *21*(12), 4192. https://doi.org/10.3390/s21124192

Cozzens, T. (2020). GPS IIR/IIR-M satellite antenna patterns released for worldwide use. *GPS World*. https://www.gpsworld.com/gps-iir-iir-m-satellite-antenna-patterns-released-for-worldwide

Donaldson, J. E., Parker, J. J. K., Moreau, M. C., Highsmith, D. E., & Martzen, P.D. (2020). Characterization of on-orbit GPS transmit antenna patterns for space users. *NAVIGATION, 67*(2), 411–438. https://doi.org/10.1002/navi.361

Federal Aviation Administration (FAA). (2005). *Category I: Local area augmentation system ground facility* (NON-FED Specification FAA-E-AJW44-2937A). Department of Transportation. https://documents.pub/document/united-states-department-of-transportation-federal-faa-e-ajw44-2937a-october-21.html?page=1

Falcone, M., Hahn, J., & Burger, T. (2017). Galileo. In P. J. G. Teunissen & O. Montenbruck (eds.), *Handbook of Global Navigation Satellite Systems* (pp. 247–272). Springer. https://doi.org/10.1007/978-3-319-42928-1_9

Fisher, S. C., & Ghassemi, K. (1999). GPS IIF – the next generation. *Proc. of the IEEE, 87*(1), 24–47. https://doi.org/10.1109/5.736340

Gatti, G., Falcone, M., Alpe, V., Malik, M., Burger, T., Rapisarda, M., & Rooney, E. (2008). GIOVE-B Chibolton in-orbit test: Initial results from the second Galileo satellite. *Inside GNSS*, 30–35. https://www.insidegnss.com/auto/sepoct08-malik.pdf

IS-GPS-200M (2021). *NAVSTAR GPS space segment/navigation user interfaces* (Revision M.). Global Positioning Systems Directorate Systems Engineering & Integration. https://www.gps.gov/technical/icwg/IS-GPS-200M.pdf

Hegarty, C. J. (2017). The global positioning system (GPS). In P. J. G. Teunissen & O. Montenbruck (eds.), *Handbook of Global Navigation Satellite Systems* (pp. 197–218). Springer. https://doi.org/10.1007/978-3-319-42928-1_7

Johnston, G., Riddell, A., & Hausler, G. (2017). The international GNSS service. In P. J. G. Teunissen & O. Montenbruck (eds.), *Handbook of Global Navigation Satellite Systems* (pp. 967–982). Springer. https://doi.org/10.1007/978-3-319-42928-1_33

Langley, R. B., Teunissen, P. J. G., & Montenbruck, O. (2017). *Introduction to GNSS*. In P. J. G. Teunissen & O. Montenbruck (eds.), *Handbook of Global Navigation Satellite Systems* (pp. 3–23). Springer. https://doi.org/10.1007/978-3-319-42928-1_1

Lee, J., Morton, Y. T. J., Lee, J., Moon, H. -S., & Seo, J. (2017). Monitoring and mitigation of ionospheric anomalies for GNSS-based safety critical systems: A review of up-to-date signal processing techniques. *IEEE Signal Processing Magazine, 34*(5), 96–110. https://doi.org/10.1109/MSP.2017.2716406

Maqsood, M., Gao, S., & Montenbruck, O. (2017). Antennas. In P. J. G. Teunissen & O. Montenbruck (eds.), *Handbook of Global Navigation Satellite Systems* (pp. 505–534). Springer. https://doi.org/10.1007/978-3-319-42928-1_17

Marquis, W., & Shaw, M. (2011). Design of the GPS III space vehicle. *Proc. of the 24th International Technical Meeting of the Satellite Division of the Institute of Navigation (ION GNSS 2011),* Portland, OR, 3067–3075. https://www.ion.org/publications/abstract.cfm?articleID=9863

Marquis, W. A., & Reigh, D. L. (2015). The GPS Block IIR and IIR-M broadcast L-band antenna panel: Its pattern and performance. *NAVIGATION, 62*(4), 329–347. https://doi.org/10.1002/navi.123

Marquis, W. A. (2016). The GPS IIR antenna panel pattern and its use on-orbit. *Proc. of the 29th International Technical Meeting of the Satellite Division of the Institute of Navigation (ION GNSS+ 2016),* Portland, OR, 2896–2909. https://doi.org/10.33012/2016.14596

Montenbruck, O., Schmid, R., Mercier, F., Steigenberger, P., Noll, C. Fatkulin, R., Kogure, S., & Ganeshan, A. S. (2015). GNSS satellite geometry and attitude models. *Advances in Space Research, 56*(6), 1015–1029. https://doi.org/10.1016/j.asr.2015.06.019

Montenbruck, O., Steigenberger, P., Prange, L., Deng, Z., Zhao, Q., Perosanz, F., Romero, I., Noll, C., Sturze, A., Weber, G., Schmid, R., MacLeod, K., & Schaer, S. (2017). The Multi-GNSS experiment (MGEX) of the International GNSS Service (IGS) – achievements, prospects, and challenges. *Advances in Space Research, 59*(7), 1671–1697. https://doi.org/10.1016/j.asr.2017.01.011

Pagot, J. -B., Julien, O., Thevenon, P., Fernandez, F. A., & Cabantous, M. (2016). Signal quality monitoring for new GNSS signals. *NAVIGATION,* 65(1), 83–97. https://doi.org/10.1002/navi.218

Pullen, S., Joerger, M. (2021). GNSS integrity and Receiver Autonomous Integrity Monitoring (RAIM). In Y. T. J. Morton, F. van Diggelen, J. J. Spilker Jr., B. W. Parkinson, S. Lo, & G. Gao (eds.), *Position, Navigation, and Timing Technologies in the 21st Century: Integrated Satellite Navigation, Sensor Systems, and Civil Applications* (Vol. 1, pp. 591–617). Wiley.

Ruf, C., Unwin, M., Dickinson, J., Rose, R., Rose, D., Vincent, M., & Lyons, A. (2013). CYGNSS: Enabling the future of hurricane prediction [remote sensing satellites]. *IEEE Geoscience and Remote Sensing Magazine, 1*(2), 52–67. https://doi.org/10.1109/MGRS.2013.2260911

Spacek, J., & Kovar, P. (2007). GNSS signal monitoring station. *2007 International Conference Radioelektronika*, Brno, Czech Republic. https://doi.org/10.1109/RADIOELEK.2007.371650

Steigenberger, P., Thoelert, S., & Montenbruck, O. (2018). GNSS satellite transmit power and its impact on orbit determination. *Journal of Geodesy,* 92, 609–624. https://doi.org/10.1007/s00190-017-1082-2

Steigenberger, P., Thoelert, S., & Montenbruck, O. (2019). Flex power on GPS Block IIR-M and IIF. *GPS Solutions,* 23. https://doi.org/10.1007/s10291-018-0797-8

Steigenberger, P., Thoelert, S., Esenbuga, O., Hauschild, A., Montenbruck O. (2020). The new flex power mode: From GPS IIR-M and IIF satellites with extended coverage area. *Inside GNSS, 15*(3), 52–56. https://insidegnss.com/the-new-flex-power-mode-from-gps-iir-m-and-iif-satellites-with-extended-coverage-area

Thoelert, S., Erker, S., & Meurer, M. (2009). GNSS signal verification with a high gain antenna – Calibration strategies and high quality signal assessment. *Proc. of the 2009 International Technical Meeting of the Institute of Navigation,* Anaheim, CA, 289–300. https://www.ion.org/publications/abstract.cfm?articleID=8312

Thoelert, S., Meurer, M., Erker, S. (2012). In-orbit analysis of antenna pattern anomalies of GNSS satellites. *NAVIGATION, 59*(2), 135–144. https://www.ion.org/publications/abstract.cfm?articleID=102573

Thoelert, S., Steigenberger, P., Montenbruck, O., & Meurer, M. (2019). Signal analysis of the first GPS III satellite. *GPS Solutions,* 23. https://doi.org/10.1007/s10291-019-0882-7

Thoelert, S., Circiu, M. -S., & Meurer, M. (2020). Impact of satellite biases on the position in differential MFMC applications. *Proc. of the 2020 International Technical Meeting of the Institute of Navigation,* San Diego, CA, 222–235. https://doi.org/10.33012/2020.17138

Thombre, S., Zahidul, M., Bhuiyan, H., Eliardsson, P., Grabrielsson, B., Pattinson, M., Dumville, M., Fryganiotis, D., Hill, S., Manikundalam, V., Poloskey, M., Lee, S., Ruotsalainen, L., Soderholm, S., & Kuusniemi, H. (2018). GNSS threat monitoring and reporting: Past, present, and a proposed future. *The Journal of Navigation, 71*(3), 513–529. https://doi.org/10.1017/S0373463317000911

van Graas, F., & Ugazio, S. (2021). GNSS signal quality monitoring. In Y. T. J. Morton, F. van Diggelen, J. J. Spilker Jr., B. W. Parkinson, S. Lo, & G. Gao (eds.), *Position, Navigation, and Timing Technologies in the 21st Century: Integrated Satellite Navigation, Sensor Systems, and Civil Applications* (Vol. 1, pp. 591–617). Wiley.

Walter, T. (2017). Satellite based augmentation systems. In P. J. G. Teunissen & O. Montenbruck (eds.), *Handbook of Global Navigation Satellite Systems* (pp. 339–360). Springer. https://doi.org/10.1007/978-3-319-42928-1_12

Wang, T., Ruf C. S., Block, B., McKague, D. S., & Gleason, S. (2019a). Design and performance of a GPS constellation power monitor system for improved CYGNSS L1B calibration. *IEEE Journal of Selected Topics in Applied Earth Observations and Remote Sensing*, *12*(1), 26–36. https://doi.org/10.1109/JSTARS.2018.2867773

Wang, T., Ruf, C. S., Gleason, S., Block, B., McKague, D., & O'Brien, A. (2019b). A real-time EIRP Level 1 calibration algorithm for the CYGNSS mission using zenith measurements. *2019 IEEE International Geoscience and Remote Sensing Symposium,* Yokohama, Japan, 8725–8728. https://doi.org/10.1109/IGARSS.2019.8900456

Wang, Y., & Shen, J. (2020). Real-time integrity monitoring for a wide area precise positioning system. *Satellite Navigation,* 1. https://doi.org/10.1186/s43020-020-00018-8

Yang, X., Wang, Q., & Xue, S. (2019). Random optimization algorithm on GNSS monitoring stations selection for ultra-rapid orbit determination and real-time satellite clock offset estimation. *Mathematical Problems in Engineering*. https://doi.org/10.1155/2019/7579185

How to cite this article: Allende-Alba, G., Thoelert, S., & Caizzone, S. (2022). Gain pattern reconstruction of GPS satellite antennas using a global receiver network. *NAVIGATION, 69*(3). https://doi.org/10.33012/navi.530